PAPER

Cascade transformations of (±)-citronellal to menthol over extruded Ru-MCM-41 catalysts in a continuous reactor†

Zuzana Vajglová,[a] Narendra Kumar,[a] Markus Peurla,[b] Kari Eränen,[a] Päivi Mäki-Arvela [ID][a] and Dmitry Yu Murzin [ID] *[a]

Cascade transformations of (±)-citronellal in a continuous mode were investigated over a bifunctional shaped ruthenium catalyst bearing metal clusters of the size 7–13 nm. Four types of Ru/H-MCM-41 extrudates (1.5 × 10 mm) containing 30% of Bindzil-50/80 colloidal silica binder were prepared varying in metal location and metal-to-acid ratio, while the concentration of Brønsted and Lewis acid sites and textural properties of the final extrudates were comparable. Catalytic tests were performed in the trickle-bed reactor under 70 °C, 10 bar of H_2, and the initial reactant concentration in cyclohexane 0.086 mol L^{-1} for the liquid residence time of 12.5 min. As a reactant, isopulegol, citronellol or (±)-citronellal was used. Metal location in extrudates has a significant effect on the catalytic activity and selectivity especially in terms of isopulegol isomers which content correlated with the metal-to-acid site ratio. Stereoselectivity to the desired (±)-menthol was 68–70%. The highest amount of the desired menthol, 32% yield, was obtained over extrudates where Ru was deposited on the catalytic support, *i.e.* with the shortest distance between the acid and metal sites, the lowest Brønsted acidity, the lowest Brønsted–Lewis acid sites ratio, the highest specific surface area and the narrowest range of the Ru particle size distribution.

1. Introduction

Menthol is a fine chemical, one of the most common aroma compounds with a worldwide demand of more than 25 000–30 000 metric tons per year.[1–5] Three asymmetric carbon atoms in the cyclohexane ring lead to a chiral compound exhibiting four diastereoisomeric pairs, namely (±)-menthol, (±)-neomenthol, (±)-isomenthol and (±)-neoisomenthol. Only (−)-menthol has a strong physiological cooling effect and the characteristic odour worthy to be commercially used in *i.e.* fragrances, toothpastes, foodstuffs, chewing gums, tobacco, confectionery, cosmetics as well as in pharma. The other seven isomers are typically considered less valuable.[1–3,5–9]

Synthetic (−)-menthol is mainly obtained by the industrial Takasago five step process with myrcene as the main reactant.[7,10–12] The last two steps in this process are the 'ene' cyclization of (+)-citronellal to (−)-isopulegol in the presence of Lewis acid aqueous $ZnBr_2$ catalyst. Under these conditions, up to 92% of (−)-isopulegol yield was obtained.[13,14] When the

tris(2,6-triarylphenoxy)aluminium catalyst was applied instead of $ZnBr_2$, 99% yield of (−)-isopulegol was reached with a clear shortcoming that the catalyst is destroyed with NaOH and cannot be recovered after the reaction.[11,15] The final production step is hydrogenation of (−)-isopulegol to (−)-menthol over a Ni catalyst.[7,10,11] The major drawback is environmentally unfriendly processes using a homogeneous Lewis acid catalyst, high costs and a need for catalyst separation.[3,7,10–12] One-pot citronellal transformation to menthol (Fig. 1) over heterogeneous catalyst represents a more attractive alternative due to an easy separation and reuse of the catalysts in one step.[10]

Various heterogeneous bifunctional powder catalysts, such as Pt, Pd, Cu, Zr on H-MCM-41;[9,16] Pt, Pd, Cu on SBA-15;[16] $ZnBr_2$, Ni on γ-Al_2O_3;[17] ZnX_2 (X = Cl, Br, NO_3), Ru, Pd, Cu on SiO_2;[18–20] Ni on ZrS;[12] Ni, Pd on MM, HPA-MM;[5] Pt, Pd, Ni, Ir, Ru, Zr, Ni/Zr, Pd/Zr on H-Beta zeolite,[2,3,8,9,11,18,21,22] have been tested in a batch operation mode. These studies revealed that the active metal has a significant effect on the side reactions such as hydrogenation of citronellal, dimerization of citronellal or isopulegol, and defunctionalisation. A higher metal loading leads to a higher amount of hydrogenation products, lower yields of cyclic products and lower menthol selectivity. The maximum selectivity to menthols and the defunctionalized products was increased with an increasing Si:Al ratio. Citronellal

[a] *Åbo Akademi University, Johan Gadolin Process Chemistry Centre, Biskopsgatan 8, Turku/Åbo, Finland 20500. E-mail: dmurzin@abo.fi*
[b] *University of Turku, Turku, Finland 20500*

† Electronic supplementary information (ESI) available: Catalyst preparation, chemicals, definitions, catalyst characterization data and catalytic testing data. See DOI: 10.1039/d0cy01251c

8108 | *Catal. Sci. Technol.*, 2020, **10**, 8108–8119

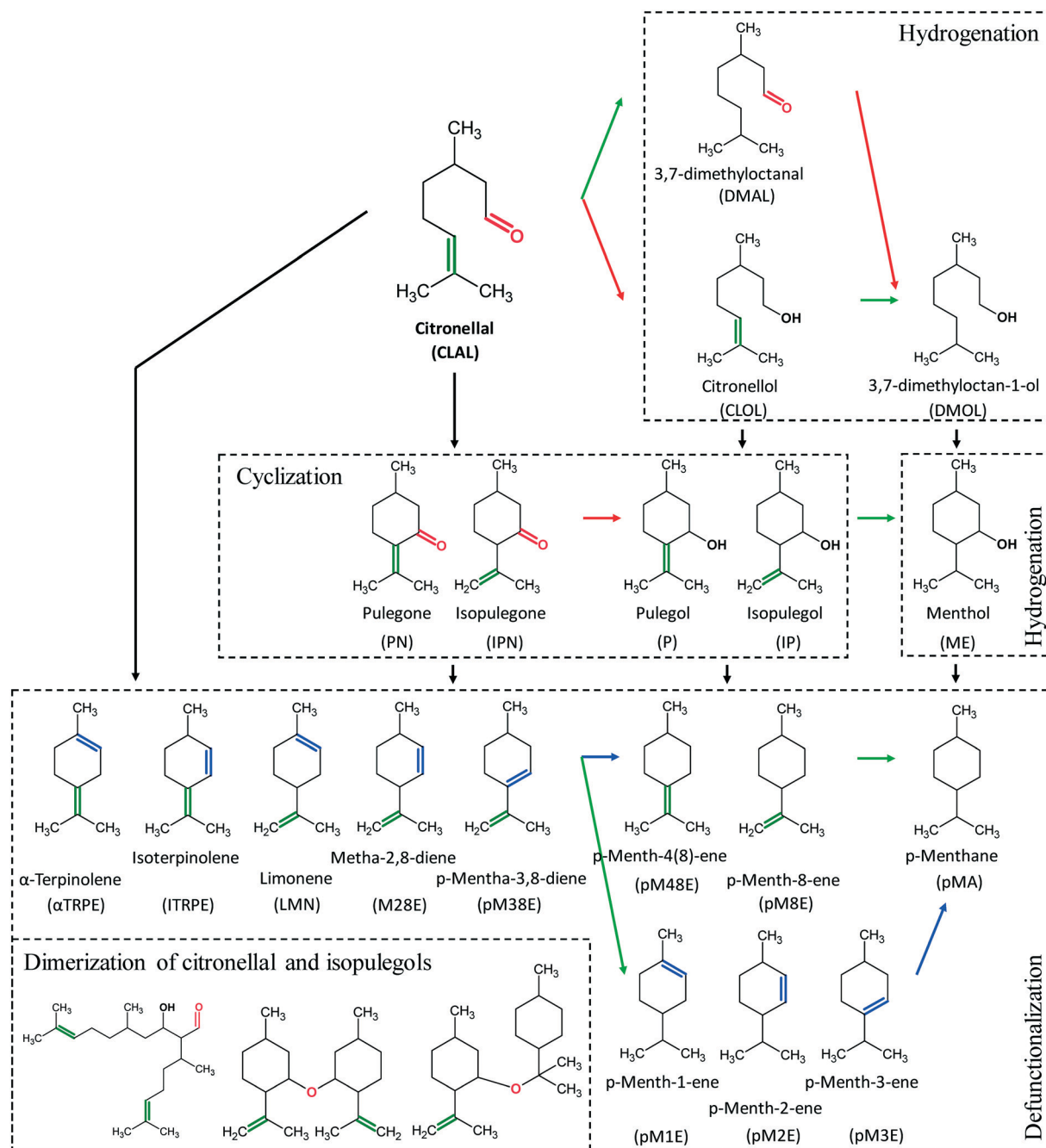This journal is © The Royal Society of Chemistry 2020

Fig. 1 Scheme of menthol synthesis from citronellal with potential side reactions.

hydrogenation is efficient at a lower temperature, while on the contrary, citronellal defunctionalisation is predominant at higher temperatures. Furthermore, the solvent has an enormous influence on the product distribution. Recently, a continuous flow tandem system for the (+)-citronellal transformation over a low cost waste-derived powder catalyst with 77% of (−)-menthol yield was reported.[1] Furthermore work of Cova et al.[23] demonstrated applicability of a waste-derived powder material, scrap ceramic-cores of automotive catalytic converters (SCATs) in the continuous-flow hydrogenation of isopulegol to menthol. Under 30 bar, 100

°C, 0.1 mL min−1 of 20 mM (−)-isopulegol in toluene, SCATs showed almost comparable (−)-menthol yield of 91.3% as a commercial 1% Pd/C catalyst (94% of yield).

However, industrially interesting is investigation of one-pot transformations over shaped catalysts in a continuous reactor, where the presence of mass transfer limitations is typically unavoidable. Such limitations can in general lead to changes in the product distribution and pronounced catalyst deactivation compared to a batch operation. The catalysts are often agglomerated with a binder to easily shape into large bodies and achieve a higher mechanical stability. Compared to a

pristine powder catalyst without a binder, physicochemical properties of the final-shaped catalysts can be significantly influenced by the binder presence, the shaping process *per se*, and chemical binder-catalyst interactions.[22,24–35]

The current work builds on our recent study of the one-pot menthol synthesis from citronellal,[22] using shaped Pt- and Ru/H-Beta catalysts with a bentonite binder in continuous flow. In that study stereoselectivity to menthol varied in the range of 67 to 73% with the undesired citronellal hydrogenation being more prominent for Pt than for Ru catalyst. While the work of Yadav and Nair[36] pointed out importance of shape selectivity in citronellal cyclization to isopulegol, there are several studies in the literature[6,10,37,38] showing that shape-selectivity is of inferior importance in comparison with the metal type and acidity in citronellal cyclization or transformations of citral to menthol. Compared to the previous work,[22] in the current study, ruthenium catalysts containing a mesoporous material H-MCM-41 and colloidal silica binder (Bindzil-50/80) without impurities were used. The mesoporous material was selected because of its large pore size compared to beta zeolites, thus allowing easier penetration of the pores without configurational diffusional limitations on one hand and on the other hand presence of lower acidity than in the zeolitic counterpart. The latter is important because too strong acidity can inevitably lead to side reactions, such as deoxygenation and catalyst deactivation. The presence of Lewis acidity in bentonite can obscure the catalytic results, thus utilization of a neutral binder – colloidal silica, gives a possibility to access the role of the catalytically active phase *per se*, without interference of the binder. Cyclohexane with a low dielectric constant and weak interactions with the surface was used as a solvent to achieve a high selectivity to menthol.[11]

This work is focused on the influence of the controlled metal location in extrudates on the mechanism, the product distribution, and catalyst deactivation and regeneration in one-pot (±)-menthol synthesis from (±)-citronellal in continuous mode.

2. Experimental

2.1. Preparation of the shaped Ru-catalysts

The procedure for shaped catalyst preparation with the controlled metal location was based on the previous work of our group.[22,24–27] This procedure included agglomeration of H-MCM-41 as a mesoporous catalytic material with Bindzil-50/80 as a colloidal silica binder, the metal introduction by incipient wetness and catalyst shaping. These synthesis steps were varied to prepare four different types of Ru-extrudates. Ru was introduced either after extrusion (A), or prior to it on alternatively a mechanical mixture of the active catalyst H-MCM-41 and a binder Bindzil-50/80 (B), only on a binder Bindzil-50/80 (C) or on H-MCM-41 (D). All catalysts contained the same composition, *i.e.* 70% of H-MCM-41, 30% of the binder with the nominal metal loading of 2 wt% in the final extrudates.

Compared to the previous work with H-Beta-25 zeolite,[22,24–27] the amount of the organic binder

methylcellulose was increased from 1 wt% to 2 wt% and the weight ratio in the suspensions for extrusion was modified to 33/65/2 of the powder catalyst/distillate water/methylcellulose to achieve a smooth shaping process and mechanically stable extrudates containing H-MCM-41. The extrudates were shaped in the one-screw extrusion device (TBL-2, Tianjin Tianda Beiyang Chemical Co. Ltd., China) into cylindrical bodies by continuous passing through holes of 1.5 mm. After drying (at 100 °C for >7 h) and calcination (at 400 °C for 3 h), the extrudates were cut to a length of *ca.* 10 mm and reduced at 350 °C for 2 h.

2.1.1. H-MCM-41 catalyst powder synthesis. Na-MCM-41 mesoporous catalyst was prepared from a gel solution (details are provided in the supporting information, Tables S1 and S2†) and treated with ultrasound at 100 W and 80 Hz for 8 h constantly on. The gel was then transferred in an autoclave with a Teflon cup, and placed in an oven at 100 °C for 72 h. The catalyst was washed with distilled water until a neutral pH (7.5–8). The dry catalyst was calcined in a step calcination procedure: the initial temperature was 250 °C (held for 1 h), this was followed by an increase to 550 °C with 6.6 °C min⁻¹ ramping and holding at the final temperature for 6 h. Na-MCM-41 form of the catalyst was transformed into its corresponding proton form by ion exchange with 0.5 M ammonium chloride solution. Thereafter, washing with distilled water to remove was done. Removal of Cl⁻ was controlled by the test with an aqueous solution of AgNO₃. Subsequently the catalyst was dried in an oven and calcined according to the same program as mentioned above.

2.1.2. Ru introduction by incipient wetness impregnation. Ru catalysts with 2 wt% nominal loading in the final extrudates were prepared by the incipient wetness impregnation method[39] with an aqueous solution of RuCl₃ hydrate (one step of impregnation for the powder catalyst, and 0.07 M solution for extrudates impregnation in three successive steps). After each step of impregnation, the samples were dried in the oven at 110 °C for 17 h. Thereafter, the catalysts were reduced under hydrogen flow at the rate 40 mL min⁻¹ from ambient temperature to 350 °C with 2 °C min⁻¹ ramping, and held at the final temperature for 3 h to remove the excess of chloride.

2.2. Characterization of shaped Ru-catalysts

All four types of extrudates and Ru/(H-MCM-41 + Bindzil-50/80) powder catalyst were characterized in detail. The quantification and strength of Brønsted and Lewis acid sites (with desorption at 250–350, 350–450, and 450 °C reflecting weak, medium, and strong acid sites, respectively) were determined by Fourier transform infrared spectroscopy with pyridine as a probe molecule (FTIR, ATI Mattson FTIR Infinity Series spectrometer, quantification using the extinction factor from Emeis[40]). Ru particle size and shape were analysed by transmission electron microscopy (TEM, JEOL JEM-1400Plus). The surface morphology, size, shape and chemical composition on the extrudates surface were studied by scanning electron microscopy and energy

8110 | *Catal. Sci. Technol.*, 2020, **10**, 8108–8119

This journal is © The Royal Society of Chemistry 2020

dispersive X-ray microanalysis (SEM-EDX, Zeiss Leo Gemini 1530). Nitrogen physisorption (Micromeritics 3Flex-3500) was performed to measure the surface area, pore volume and pore size distribution. Ru concentration in the entire volume of the catalyst was analysed by inductively couple plasma – optical emission spectrometry (ICP-OES, PerkinElmer Optima 5300 DV instrument). The catalyst (about 0.1 g) was microwave digested with a mixture containing 9 mL of 37% HCl, 3 mL of 65% HNO_3 and 1 mL of 50% HBF_4. After digestion dilution to 100 mL was done using distilled water. To determine potential catalyst leaching by ICP-OES, the liquid sample of the reaction mixture after the reaction (5.5 mL) was evaporated under the flow rate of nitrogen and then diluted by 5.5 mL 1.5% HCl. Details of the physico-chemical characterization methods and equipment are presented in our previous publications.[22,24–27]

2.2.1. Catalytic tests. The continuous catalytic experiments were performed over Ru-shaped catalysts (10 × 1.4 mm) where the presence of mass transfer limitation[22,25–27] is expected as in the industrial process. The catalyst was diluted with inert quartz with the size 0.2–0.8 mm to fill the whole reactor volume for better flow distribution throughout the reactor. Formation of menthol from isopulegol (IP), citronellol (CLOL) or citronellal (CLAL) was used as model reactions to investigate the effect of the controlled metal deposition in shaped catalysts. All reactions were performed over 1 g of Ru-extrudates (A = 1.0030 g, B = 1.0013 g, C = 1.0018 g, D = 1.0005 g) in the trickle-bed reactor operating in a co-current downflow mode (ID 12.5 mm, length and volume of the catalyst bed were 102 mm and 12.5 mL, respectively)[22,25,27] under 70 °C, 10 bar of H_2, 50 mL min^{-1} of H_2, 0.4 mL min^{-1} of the feed with 0.086 mol L^{-1} of the initial reactant concentration (Table S3†) in cyclohexane with the liquid residence time of 12.5 min. A high hydrogen molar excess was applied to ensure a good distribution of the reactants across the reactor being also beneficial for mitigation of catalyst deactivation.

Analysis of the flow regimes using the flow map for trickle bed reactors[41,42] and considering low gas and liquid flow rates used in the current work confirms a trickling flow regime. The Ru-catalysts were reduced *in situ* under a hydrogen flow of 40 mL min^{-1} using the temperature ramp of 10 °C min^{-1} to 350 °C for 2 h. Before the reaction, the catalyst was wetted with 0.5 mL min^{-1} of a neat solvent for 20 min. The reaction was carried out for 3 h with sampling after every 30 min. The catalyst reuse was investigated in the following way: the catalyst was flushed in the reactor under a flow of the solvent and left under 2.5 bar of H_2 pressure overnight.

The reaction products were diluted with cyclohexane and analysed using an Agilent GC 6890 N equipped with an FID and DB-1 column (30 m × 250 μm × 0.5 μm). The temperature of the FID was 340 °C. The products were confirmed with an Agilent GC/MS 6890 N/5973 using the same column and the temperature program.

More details of catalytic tests, definitions, apparatus, equipment and analysis are presented in the supporting information and in our previous publications.[22,25,27]

3. Results and discussion

Catalyst of type B was selected as a reference catalyst and used in each model reaction in the trickle-bed reactor. In this catalyst, Ru was uniformly distributed in the entire shaped body, and deposited on both H-MCM-41 and the Bindzil-50/80 binder. All four types of Ru-extrudates were characterized in detail and catalytic results were correlated with the physico-chemical properties.

3.1. Characterization results of shaped Ru-catalyst

As in the previous study,[26] TEM analysis confirmed that different synthesis procedures resulted in the controlled metal deposition in the shaped catalysts (Table 1 and Fig. S1 and S2†). For A and B types of extrudates, random deposition of Ru on H-MCM-41 mesoporous catalytic material and Bindzil-50/80 binder was observed. For C and D extrudates, Ru was exclusively deposed on either the binder or on the mesoporous material, respectively. TEM analysis also revealed that the average Ru particle size was lower than 13 nm for all types of extrudates (d_{Ru}, Table 2). The smallest Ru particles was determined for A type extrudates (7 nm) prepared *via* the post synthesis method (Fig. S2 and S3†). Ru particle size distribution (Fig. S3†) shows a narrow range of the particle size (2–30 nm) for D extrudates with Ru locating exclusively on the H-MCM-41 and for Ru/(H-MCM-41 + Bindzil-50/80) powder catalyst. In fact such cluster size can be beneficial for a tandem reaction, as otherwise smaller catalyst size and thus higher metal dispersion can be beneficial for hydrogenation of citronellal to side products (*e.g.* citronellol and 3,7-dimethyloctan-1-ol).

Diameter of extrudates was determined to be 1.4 and 1.3 mm by SEM for the shaped bodies prepared *via* the post synthesis – A and *in situ* synthesis methods – B, C, D, respectively. SEM analysis also revealed visible holes with the diameter of 3–65 μm on the surface of extrudates (Fig. S4†). This could be attributed to the removal of methylcellulose during calcination.[22,25–27] In line with our previous studies, SEM images clearly show chemical interactions between H-MCM-41 and the Bindzil-50/80 binder, and a smooth surface of extrudates after application of the mechanical force during extrusion with a partial preservation of the individual phase structure.

A 4.4 fold higher value of Ru concentration on the top (C_{Ru_E}, Table 2) of A extrudates surface (prepared *via* the post synthesis) determined using EDX confirmed the egg-shell type of metal distribution with ruthenium located on the outmost layer of the catalyst (Table 1). This is in line with a previous study focused on Pt/H-Beta-25 extrudates containing bentonite,[26] where the actual value of Pt concentration and thickness of a penetrated Pt layer were determined to be 8.3% and 60 μm, respectively, for the same nominal loading as in the current work.

The real Ru concentration in the entire volume of catalyst determined using ICP-OES (c_{Ru}, Table 2) was almost half of the nominal loading. For catalyst C, where Ru is located exclusively on the binder, Ru concentration was the lowest one. This could be attributed to too high

This journal is © The Royal Society of Chemistry 2020

Catal. Sci. Technol., 2020, **10**, 8108–8119 | **8111**

Table 1 Shaped Ru-catalysts with the controlled metal location

Extrudates	Synthesis method	Ru distribution	Ru deposition
A	Post: shaping of a composite material, followed by Ru impregnation	At the outermost layer of extrudates	H-MCM-41, Bindzil binder
B	*In situ*: Ru impregnation of a composite material, followed by extrusion	Uniformly in the entire shaped body	H-MCM-41, Bindzil binder
C	*In situ*: deposition of Ru on a binder, synthesis with H-MCM-41, followed by extrusion	Uniformly in the entire shaped body	Bindzil binder
D	*In-situ*: deposition of Ru on H-MCM-41, synthesis with binder, followed by extrusion	Uniformly in the entire shaped body	H-MCM-41

A – Ru/(H-MCM-41 + Bindzil), post synthesis; B – Ru/(H-MCM-41 + Bindzil), *in situ* synthesis; C – (Ru/Bindzil) + H-MCM-41; D – (Ru/H-MCM-41) + Bindzil.

Table 2 Characterization results of shaped Ru-catalysts with the controlled metal location

|	TAS μmol g^{-1}	BAS μmol g^{-1}	LAS μmol g^{-1}	BAS/LAS —	d_{Ru} nm	D_{Ru} %	c_{Ru_E} %	c_{Ru} %	A m^2 g^{-1}	V_p cm^3 g^{-1}	c_{Ru}/c_{AS} —
A	60	37	24	1.53	7	14	8.8	1.2	483	0.65	0.29
B	51	31	21	1.49	13	8	1.2	1.2	514	0.72	0.17
C	60	35	25	1.38	11	9	0.3	0.9	502	0.67	0.14
D	52	29	22	1.31	10	10	1.6	1.2	520	0.71	0.23

A – Ru/(H-MCM-41 + Bindzil), post synthesis; B – Ru/(H-MCM-41 + Bindzil), *in situ* synthesis; C – (Ru/Bindzil) + H-MCM-41; D – (Ru/H-MCM-41) + Bindzil; BAS – Brønsted acid sites; LAS – Lewis acid sites; TAS – total acid sites; d_{Ru} – Ru particle size; D_{Ru} – metal dispersion ($100/d_{Ru}$); c_{Ru_E} – Ru concentration on the top of extrudates surface; c_{Ru} – Ru concentration in the entire volume; A – specific surface area; V_p – specific pore volume; c_{AS} – concentration of total acid sites.

Ru loading on the binder, with the latter accounting for only 30% of the entire extrudate.

In line with the previous studies,[22,26] the concentration of Brønsted and Lewis acid sites and textural properties of the final extrudates (Table 2, Fig. 2 and Table S4†) are comparable with each other without being significantly affected by different preparation steps. Extrudates contained *ca.* 20% and 80% of the micro- and mesopore volume, with respective sizes at maximum of 0.7 and 3.4 nm. Micropore volume was the same (0.14 cm^3 g^{-1}) for all extrudates.

3.2. Activity and selectivity of shaped Ru-catalysts in one-pot transformations

3.2.1. Isopulegol as a reactant. Fig. S5† shows conversion of isopulegol, the liquid phase mass balance closure, the total yield, and the product yields as a function of time-on-stream (TOS). The transient behaviour, characterizing dynamics of the processes in the reactor, was observed in the first 1.5 h, where the liquid phase mass balance closure increased from 6 to 81%. During this transient period, an intermediate *p*-menthane was observed with 0.8% of the maximum yield at
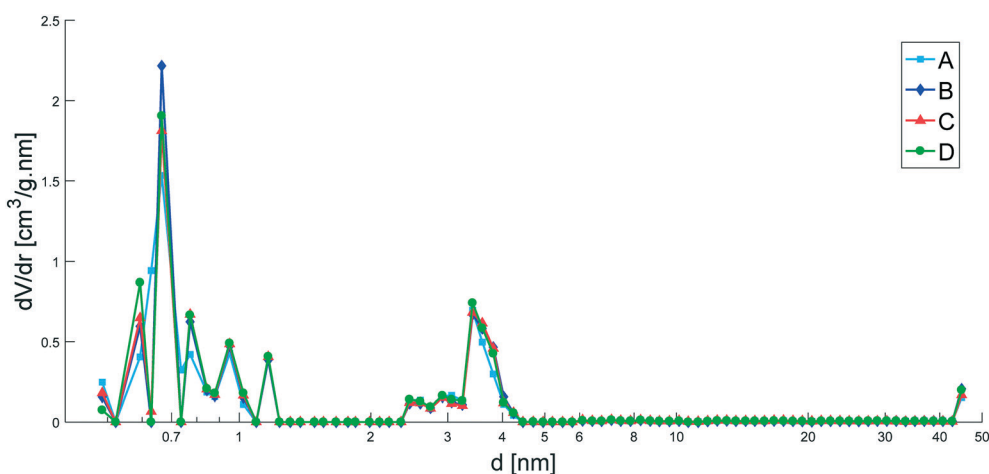
Fig. 2 Pore size distribution. Legend: A – Ru/(H-MCM-41 + Bindzil), post synthesis (light blue square); B – Ru/(H-MCM-41 + Bindzil), *in situ* synthesis (dark blue diamond); C – (Ru/Bindzil) + H-MCM-41 (red triangle); D – (Ru/H-MCM-41) + Bindzil (green circle).

8112 | *Catal. Sci. Technol.*, 2020, **10**, 8108–8119

This journal is © The Royal Society of Chemistry 2020

30 min. After 2 h of TOS, a slight decline of conversion was observed (by 3.5% per hour) with steady state yields of products. After 3 h of TOS with 12.5 min of the residence time, the conversion of isopulegol was 86% with the liquid phase mass balance closure of 88% and the total yield of 74% over Ru/(H-MCM-41 + Bindzil), i.e. the catalyst of type B, where Ru was deposited on a powder mixture of MCM-41 and the binder, followed by extrusion. Only menthols were present in the final reaction mixture. The yields of menthol and neo-menthol were 73.3% and 0.5%, respectively. The initial reaction rate and turnover frequency (TOF) were 5.7×10^{-7} mol g^{-1} s^{-1} and 0.0049 s^{-1}, respectively (Table S5†).

Compared with the literature,[43] a similar isopulegol conversion (84%) and a slightly higher mass balance (95%) were obtained after 16 h using 50 mg of 0.74% Pt/W-TUD-1 catalyst with 9 wt% of WO$_3$ at 80 °C and 20 bar H$_2$ in a batch reactor. The initial reaction rate and TOF were in this case 1.2×10^{-6} mol g^{-1} s^{-1} and 0.031 s^{-1}, respectively. Undesired acid catalysed dehydroxylation was not observed.

3.2.2. Citronellol as a reactant. Fig. S6† displays the same type of catalytic data as for isopulegol hydrogenation. Similar transient behaviour was observed as in the case discussed above, including an increase of the liquid phase mass balance closure (from 4 to 100% in 2 h) with TOS. After 2 h of TOS, the steady state was achieved. In the first 1 h of TOS, menthols and isopulegols were observed with less than 2.5% of yield. After 3 h of time-on-stream, conversion of citronellol reached 96% with the liquid phase mass balance closure of 100% and the total yield for 96% over Ru/(H-MCM-41 + Bindzil), i.e. catalyst of type B. Only 3,7-dimethyloctan-1-ol (DMOL) was present in the final reaction mixture. This is in line with literature focusing on citronellal transformation over Ru/H-Beta catalyst[3,9] where it was stated, that hydrogenation of the C=C bond in citronellol results in DMOL.

Results (Fig. S6†) clearly show that hydrogenation route was predominated at the expense of citronellol cyclization. This behaviour can be explained by absence of the C=O bond. The initial reaction rate and TOF were 4.9×10^{-7} mol g^{-1} s^{-1} and 0.0043 s^{-1}, respectively (Table S5†).

3.2.3. Citronellal as a reactant. All four types of extrudates (Table 1) were tested in the menthol synthesis from (±)-citronellal (Fig. 3 and Table 3). Significant differences were observed in the citronellal conversion (87–96%), liquid phase mass balance closure (56–69%) and the product distribution (Fig. 4). In contrast, the catalysts showed similar total yields (50–54%) after 3 h of TOS (Fig. 3c), which can be related to a narrow range of Lewis acid sites (21–25 µmol g^{-1}) (Fig. 5a).

Citronellal conversion of 98% was obtained in a batch reactor over 3 wt% Ru/H-Beta powder catalyst without a binder at 80 °C, 15 bar H$_2$ and with cyclohexane as a solvent within 10 h (ref. 11) as for the D catalyst (where Ru was exclusively deposited on H-MCM-41, X = 96.2%, Table 3). Compared to our previous work,[22] more than 10% lower citronellal conversion (75–79%), ca. 2-fold lower total yield (25–33%) and a similar liquid phase mass balance closure (52–68%) were obtained over Ru/H-Beta-25 extrudates containing bentonite binder at a lower reaction temperature (35 °C) in a continuous reactor. The observed decline of conversion due to deactivation was comparable for all tested in than work Pt-, Ru extrudates bearing H-Beta-25 zeolite.[22]

In the current work, a slight decline of conversion was revealed for the catalysts where Ru was deposited exclusively on H-MCM-41 (by 3.0% in 3 h, D catalyst) or on Bindzil-50/80 binder (by 6.5% in 3 h, C catalyst), while catalysts with randomly deposited Ru showed a significant decline in conversion (by 13.0 and 15.2% in 3 h for A extrudates prepared via the post synthesis method and B extrudates prepared via the so-called in situ synthesis method, respectively).

In the literature,[43] some polymerization and coking, i.e. accumulation of organic compounds inside the catalyst, were proposed as a reason for possible deactivation when Pt catalyst was used in a batch reactor operating at 80 °C, 20 bar H$_2$ with toluene as a solvent.

Some linear correlations visible in Fig. 5 especially using the ratio between metal and acid sites as a parameter reflect the dual nature of the cascade transformation of citronellal to menthol comprising metal catalyzed hydrogenation reactions and acid catalyzed cyclization.

The highest amount of the desired menthol (32.1% of yield, Fig. 6 and Table S6†) was obtained over D extrudates where Ru was deposited on the catalytic support, i.e. with the shortest distance between the acid and metal sites, the lowest Brønsted acidity, the lowest Brønsted–Lewis acid sites ratio, the highest specific surface area and the narrowest range of the Ru particle size distribution. In contrast, the lowest amount of the desired menthol (21.8% of yield, Fig. 6 and
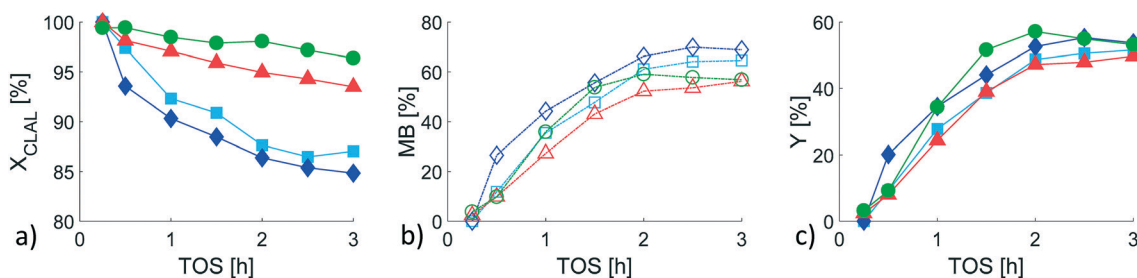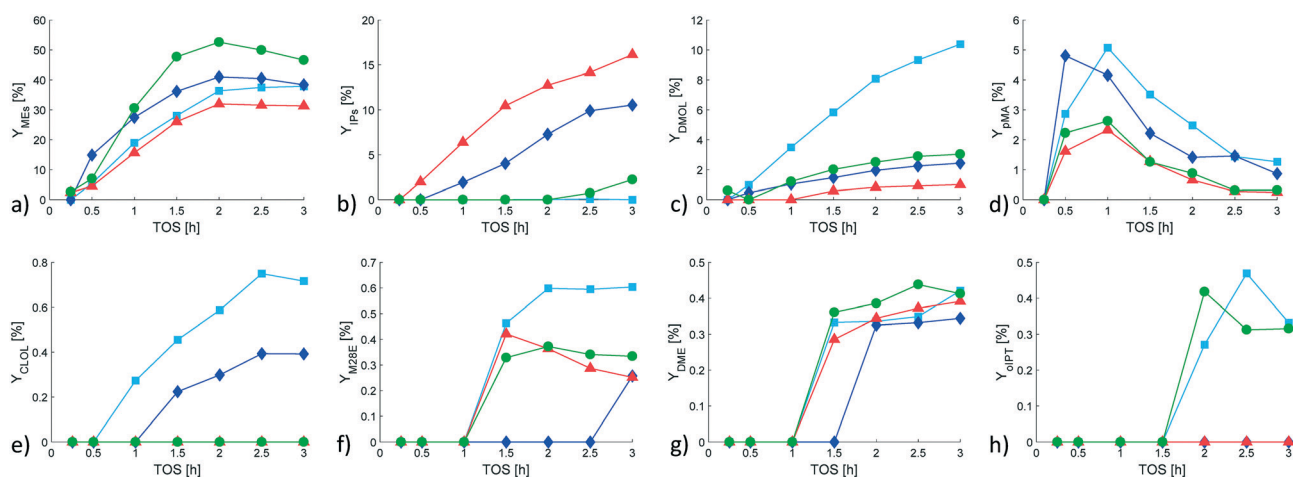

Fig. 3 Menthol synthesis from (±)-citronellal: a) conversion, b) liquid phase mass balance closure, c) total yield. Legend: A – Ru/(H-MCM-41 + Bindzil), post synthesis (light blue square); B – Ru/(H-MCM-41 + Bindzil), in situ synthesis (dark blue diamond); C – (Ru/Bindzil) + H-MCM-41 (red triangle); D – (Ru/H-MCM-41) + Bindzil (green circle).

This journal is © The Royal Society of Chemistry 2020

Catal. Sci. Technol., 2020, **10**, 8108–8119 | **8113**

Table 3 The results from menthol synthesis from (±)-citronellal after 3 h of TOS. The values are given in percentage

| | X | MB | Y | Y_{ACP} | Y_{CP} | Y_{DM} | Y_{DFP} | Y_{MEs} | Y_{IPs} | ACP | | | DFP | | | |
										Y_{CLOL}	Y_{DMOL}	Y_{DME}	Y_{M28E}	Y_{pMA}	Y_{pM138E}	Y_{oIPT}
A	87.0	64.6	51.6	11.5	40.1	0.0	2.2	37.9	0.0	0.7	10.4	0.4	0.6	1.3	0.03	0.3
B	84.8	68.9	53.7	3.2	50.5	0.0	1.6	38.4	10.5	0.4	2.4	0.3	0.3	0.9	0.0	0.0
C	93.5	56.2	49.7	1.4	48.3	0.0	0.9	31.3	16.1	0.0	1.0	0.4	0.3	0.2	0.0	0.0
D	96.4	56.8	53.2	3.4	49.8	0.0	1.0	46.6	2.2	0.0	3.0	0.4	0.3	0.3	0.0	0.3
B^{II}	84.9	71.2	56.2	3.6	52.6	0.0	1.3	32.6	18.7	0.6	2.4	0.3	0.3	0.0	0.4	0.0
B^{III}	83.4	70.8	54.3	3.8	50.4	0.0	1.3	30.8	18.3	0.7	2.6	0.4	0.3	0.0	0.4	0.0

X – conversion, MB – liquid phase mass balance closure, Y – total yield, Y_{ACP} – yield of acyclic hydrogenation products, Y_{CP} – yield of cyclic products (MEs + IPs + DFP), Y_{DM} – yield of dimeric ethers and heavy components, Y_{DFP} – yield of defunctionalization products, Y_{MEs} – yield of menthols, Y_{IPs} – yield of isopulegols, Y_{CLOL} – yield of citronellol, Y_{DMOL} – yield of 3,7-dimethyloctan-1-ol, Y_{DME} – 2,6-dimethyloctane, Y_{M28E} – yield of metha-2,8-diene, Y_{pMA} – yield of *p*-menthane, Y_{pM138E} – yield of *p*-mentha-1,3,8-triene, Y_{oIPT} – yield of *o*-isopropyltoluene; A – Ru/(H-MCM-41 + Bindzil-50/80), post synthesis; B – Ru/(H-MCM-41 + Bindzil-50/80), *in situ* synthesis; C – (Ru/Bindzil-50/80) + H-MCM-41, *in situ* synthesis; D – (Ru/H-MCM-41) +Bindzil-50/80, *in situ* synthesis; B^{II} – reused II B – Ru/(H-MCM-41 + Bindzil-50/80), *in situ* synthesis; B^{III} – reused III B – Ru/(H-MCM-41 + Bindzil-50/80), *in situ* synthesis.

Fig. 4 Product distribution in menthol synthesis from (±)-citronellal: a) menthols, b) isopulegols, c) 3,7-dimethyloctan-1-ol, d) *p*-menthane, e) citronellol, f) metha-2,8-diene, g) 2,6-dimethyloctane, h) *o*-isopropyltoluene. Legend: A – Ru/(H-MCM-41 + Bindzil), post synthesis (light blue square); B – Ru/(H-MCM-41 + Bindzil), *in situ* synthesis (dark blue diamond); C – (Ru/Bindzil) + H-MCM-41 (red triangle); D – (Ru/H-MCM-41) + Bindzil (green circle).
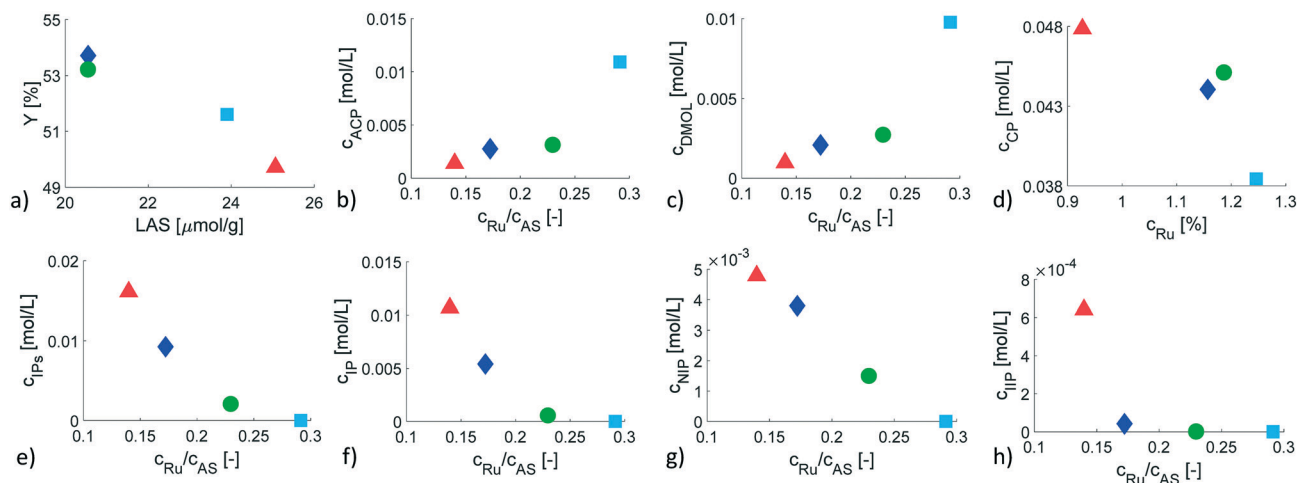
Table S6†) was obtained over C extrudates where Ru was deposited on the binder, *i.e.* the material bearing the second-longest distance between the acid and metal sites, the highest Lewis acidity, the lowest metal-to-acid site ratio, and the lowest Ru concentration.

Furthermore, it was observed that the ratio of the menthol isomers (menthol/neomenthol/isomenthol/neoisomenthol) was the same (namely 69/24/1/6) (Fig. 6 and Table S6†) while the ratio of the isopulegol isomers was significantly different (0–66)/(0–73)/(0–4)/0 of isopulegol/neoisopulegol/isoisopulegol/neoisopulegol (Fig. S7 and Table S7†) for all four types of catalyst containing the same composition. During the reaction, the stereoisomeric ratio was changed (Fig. S7†). Such results in general can be explained either by interconversion between different isopulegols or by different rates of the hydrogenation to menthols. A latter explanation implies that the ratio of menthols will be also changing, which is apparently not the case. The observed behaviour is different from the results

reported in the literature,[2,11] where a constant isopulegols ratio during the reaction time was obtained.

Overall, distribution of the four isopulegol diastereomers obtained in citronellal cyclization can strongly depend on the catalyst.[3] About 70–75% of stereoselectivity to (±)-isopulegol is typical for an acid solid catalyst such as zeolite adhering to the thermodynamic equilibrium[2,3,8,10,11,44] while a higher (±)-isopulegol stereoselectivity of *ca.* 90–94% was achieved with Lewis acids catalysts such as ZnBr$_2$ or Zr-Beta.[3,11,44] Stereoselectivity to (±)-isopulegol of 61–65% obtained in hydrogenation of citronellal over Ru-extrudates[22] is comparable with values observed for B and C catalysts in the current work. In the case of A catalyst, no isopulegols were obtained similar to Pt-extrudates.[22] In all cases,[2,3,8,10,11,22,44] the desired stereoisomer (±)-isopulegol was obtained as the predominant one. This is not in line with the behaviour of D catalyst, where (±)-neoisopulegol was observed as the predominant isomer with 73% of stereoselectivity. Formation of individual isopulegols, as well as the sum of isopulegols,

8114 | *Catal. Sci. Technol.*, 2020, **10**, 8108–8119

This journal is © The Royal Society of Chemistry 2020

Fig. 5 Menthol synthesis from (±)-citronellal after 3 h: a) the total yield as a function of the Lewis acid sites; b and c) the concentration of acyclic hydrogenation products and concentration of 3,7-dimethyloctan-1-ol as a function of the metal-to-acid sites ratio; d) the concentration of cyclic products as a function of Ru concentration; e–h) the concentration of isopulegols, (±)-isopulegol, (±)-neoisopulegol, (±)-isoisopulegol as a function of the metal-to-acid sites ratio. Legend: A – Ru/(H-MCM-41 + Bindzil), post synthesis (light blue square); B – Ru/(H-MCM-41 + Bindzil), *in situ* synthesis (dark blue diamond); C – (Ru/Bindzil) + H-MCM-41 (red triangle); D – (Ru/H-MCM-41) + Bindzil (green circle).
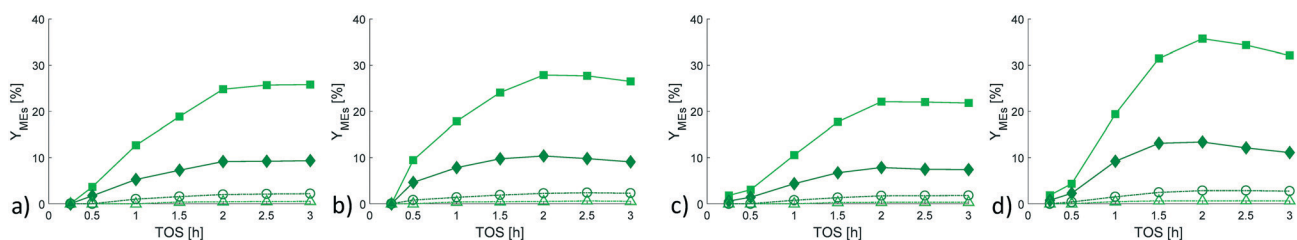
Fig. 6 Menthol isomers as a function of time-on-stream in menthol synthesis from (±)-citronellal over: a) A – Ru/(H-MCM-41 + Bindzil-50/80), post synthesis; b) B – Ru/(H-MCM-41 + Bindzil-50/80), *in situ* synthesis; c) C – (Ru/Bindzil-50/80) + H-MCM-41, *in situ* synthesis; d) D – (Ru/H-MCM-41) + Bindzil-50/80, *in situ* synthesis. Legend: menthol (ME, light green, filled square), neomenthol (NME, dark green, filled diamond), isomenthol (IME, light green, empty triangle), neoisomenthol (NIME, dark green, empty circle).

can be correlated with the metal-to-acid site ratio (c_{Ru}/c_{AS}) (Fig. 5e–h). In the case of (±)-neoisopulegol, a linear dependence was observed while (±)-isopulegol and (±)-isoisopulegol increased exponentially with decreasing the c_{Ru}/c_{AS} ratio. Overall, it can be concluded that a higher metal concentration leads to a lower formation of isopulegols.

Stereoselectivity to the desired (±)-menthol of 68–70% over all Ru/H-MCM-41 extrudates containing the Bindzil binder was comparable with the literature data[22] over Ru/H-Beta-25 extrudates when bentonite was used as a binder (67–69%). For Pt-catalyst a slightly higher (±)-menthol stereoselectivity was obtained (71–76%).[8,22] A significantly higher (±)-menthol stereoselectivity of 84%, >85% and 93% were achieved over Fe/SCATs,[1] Ru–ZnBr$_2$/SiO$_2$ (ref. 18) and Zr/Beta&Ni/MCM-41 (ref. 9) catalysts, respectively, while only 60% was obtained for Ni/ZrS (ref. 12) catalyst. In all cases, the desired (±)-menthol stereoisomer was obtained as the predominant one and the menthols ratio was stable during reactions performed in a batch mode.

For D catalyst with the highest amount of the desired (±)-menthol, the total yield of menthols (MEs), the total yield of isopulegols (IPs), the yield of acyclic hydrogenation products (ACP) and defunctionalized products (DFP) was 46.6%, 2.2%, 3.4% and 1%, respectively (after 3 h of TOS with the residence time of 12.5 min, 70 °C, 10 bar H$_2$, cyclohexane). Compared to H-Beta-25-bentonite extrudates where Ru was also exclusively deposited on the support, 5-fold higher yield of IPs, along with 3-fold and 17-fold lower yields of MEs and ACP, respectively, were obtained at 35 °C, 10 bar H$_2$ in a continuous mode with cyclohexane as a solvent.[22]

In a batch reactor over 3 wt% Ru/H-Beta powder catalyst without a binder at 80 °C, 15 bar,[11] *ca.* 8-fold higher yield of IPs, 2-fold and 18-fold lower yields of MEs and ACP, respectively, were observed compared to the catalyst D. It should be also pointed out that the results are not directly comparable because of different reaction conditions, metal concentration and the catalyst support. A similar yield of MEs (43%) as for D catalyst was achieved over 2 wt% Ru/H-Beta powder catalyst bearing clusters of the size 1.4 nm without a binder in a batch reactor within 40 min at 100 °C, 25 bar H$_2$, with *n*-hexane as a solvent, accompanied with 9-fold, 10-fold and 4-fold higher yields of IPs, ACP and DFP, respectively.[3] The yield of the dimerization products was calculated to be 1%. As an acyclic hydrogenation product

This journal is © The Royal Society of Chemistry 2020

Catal. Sci. Technol., 2020, **10**, 8108–8119 | **8115**

citronellal was detected, followed by its consecutive hydrogenation to 3,7-dimethyloctan-1-ol. Among defunctionalized products the largest fraction was observed for *p*-mentenes and *p*-menthanes.[2,3] Except for dimerization products, this is in line with the results obtained in the current work. Azkaar *et al.*[22] and Neatu *et al.*[11] did not mention formation of any defunctionalized products.

Furthermore, it was observed that selectivity to menthols increased with an increasing particle size in the batch reactor[3] while for Pt- and Ru-extrudates in a continuous reactor, the opposite trend was noticed.[22] However, in the current work, apparently no correlations between selectivity to menthols and the ruthenium particle size could be seen.

In the current work, *p*-menthane was observed as an intermediate with the maximum up to 1 h of TOS for all catalyst types (Fig. 4). The most prominent maxima in *p*-menthane formation were observed for A and B extrudates with random deposition of ruthenium and the highest Brønsted-to-Lewis acid sites ratio (BAS/LAS, Table 2). As other intermediates *o*-isopropenyltoluene with the maximum at 2–2.5 h of TOS only for A and D extrudates, and mentha-2,8-diene with the maximum at 1.5 h of TOS for C extrudates were detected (Fig. 4). The yields of other products identified in the reaction mixture (menthols; isopulegols; 3,7-dimethyloctan-1-ol and 2,6-dimethyloctane) increased with increasing time-on-stream for all catalysts. Moreover, the yields of citronellol and mentha-2,8-diene were increasing with increasing TOS over A, B and A, B, D extrudates, respectively (Fig. 4). A significant difference was observed for formation of isopulegols (IPs) and menthols (MEs) for all catalysts, and for formation of 3,4-dimethyloctan-1-ol (DMOL) for A catalyst. Compared to other catalysts, *ca.* 5-fold higher amount of DMOL was obtained over A extrudates. That can be attributed to the highest metal-to-acid site ratio (c_{Ru}/c_{AS}) (Fig. 5b and c) and a shorter diffusional distance due to the egg-shell structure, where the active metal is concentrated on the outermost layer of the extrudates. This most probably promotes further hydrogenation at the expense of cyclization. On contrary, for catalysts where the diffusion distance was longer, *i.e.* Ru was homogeneously distributed along the entire shaped body (B, C, D extrudates), the results revealed that the yield of isopulegols decreased (C > B > D, Table 3 and Fig. 4b and S7†) and the yield of menthols increased (C < B < D, Table 3 and Fig. 4a and 6) with the decreasing distance between acid and metal sites (C > B > D, Fig. S1†).

Overall, the concentration of acyclic hydrogenation products (ACP) and cyclic products (CP) increased with TOS (Fig. 7a). The concentration of ACP was significantly higher over extrudates A compared to other extrudates (Fig. 7a and S8a†) which can be explained by the highest metal dispersion in this case in accordance to the literature.[3] On the other hand, the concentration of cyclic products was comparable to each other, being only slightly lower for A (Fig. 7b). Neither dimeric ethers nor heavy components were observed in the reaction mixtures. The initial ratio between acyclic hydrogenation products to cyclic products increased 2.7, 2.4,

1.9 and 1.3-fold for B, A, D and C catalyst, respectively, after 3 h of TOS (Fig. 7c). The highest increase of the ACP/CP ratio as well as the isopulegols/menthols ratio (Fig. 7d) was thus observed for the catalyst of type of B, where the Ru was deposited randomly on both H-MCM-41 and Bindzil binder.
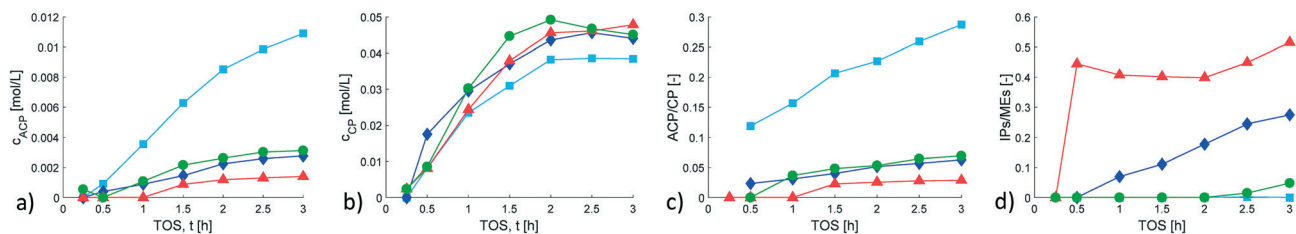
Furthermore, the results showed that the concentration of acyclic hydrogenation products decreased with increasing concentration of cyclic products (Fig. S8a†) and at the same time decreasing concentration of *p*-menthane, *p*-menthene and *p*-menthadiene (Fig. S8b†). In line with the literature,[18] the concentration of cyclic products, especially concentration of isopulegols decreased with increasing Ru concentration (Fig. 5d), which can be explained as a result of more prominent hydrogenation to 3,7-dimethyloctan-1-ol. Concentration of isopulegols decreased with increasing concentration of menthols as a result of consecutive hydrogenation (Fig. S8c†) obviously except the catalyst A where no isopulegols were detected. Concentration of menthols and isopulegols increased with decreasing concentrations of defunctionalized products such as *p*-menthane, *p*-menthene, *p*-menthadiene, *p*-menthatriene, *o*-cymene and *o*-isopropenyltoluene (Fig. S8d†). Catalyst A exhibiting both the smallest Ru particles, 7 nm and a high Ru loading (Table 2) promoted dehydration of isopulegol (Fig. 8c and d). The effect of Ru loading varying from 1–4 wt% was also investigated in one-pot transformation of citronellal to menthol in the literature.[3] In that study the highest selectivity to defunctionalized products was obtained over 4 wt% Ru-H-BEA-150 with 11.1 nm Ru particles and the second highest amount with 4 wt% Ru-H-BEA-35 with the particle size of 3.7 nm. On the other hand, catalyst C in the current work exhibited Ru particles of the size 11 nm located on the binder. Furthermore, this catalyst exhibited the BAS/LAS ratio lower than catalyst A (Table 2) which led to formation of only small amounts of defunctionalized products (Fig. S8c†).

The initial reaction rates and TOF were in the range (5.85–6.42) × 10⁻⁶ mol g⁻¹ s⁻¹ and 0.0043–0.0068 s⁻¹, respectively (Table S5†). *Ca.* 3–5-fold higher value of turnover frequency obtained in the batch experiment over 2 wt% Ru/H-Beta without a binder (TOF = 0.0217 at conditions: 80 °C, 25 bar, *n*-hexane, 2.5 h) clearly confirmed presence of mass transfer limitations in extrudates.[3]

A reference catalyst B was consecutively reused two-times to elucidate catalyst deactivation (Fig. 8).

Regeneration was performed by simply washing the catalyst with cyclohexane (0.5 mL min⁻¹ for 30 min). In comparison to the fresh catalyst, negligible changes were observed in terms of citronellal conversion, liquid phase mass balance closure and the total yields obtained after 3 h of TOS (Fig. 8). On the contrary, significant changes were observed in decreasing the yields of menthols (by *ca.* 15%) and *p*-menthane, and increasing the yields of isopulegols (by *ca.* 2-fold) and citronellol after the first reuse of the catalyst (B^{II}, Fig. 8d and S9†). After the second reuse of catalyst (B^{III}), only the yield of menthols was decreased (by additional 4.7%) and the yield of citronellol was increased again indicating deactivation of acid sites. The yields of isopulegols

8116 | *Catal. Sci. Technol.*, 2020, **10**, 8108–8119

This journal is © The Royal Society of Chemistry 2020

Fig. 7 Menthol synthesis from (±)-citronellal: a) concentration of acyclic hydrogenation products, b) cyclic products, c) acyclic hydrogenation-cyclic products ratio, d) isopulegols–menthols ratio as a function of TOS. Legend: A – Ru/(H-MCM-41 + Bindzil), post synthesis (light blue square); B – Ru/(H-MCM-41 + Bindzil), *in situ* synthesis (dark blue diamond); C – (Ru/Bindzil) + H-MCM-41 (red triangle); D – (Ru/H-MCM-41) + Bindzil (green circle).
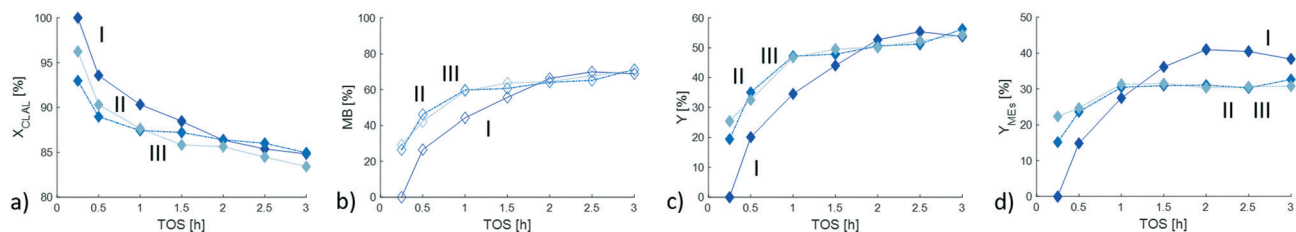
Fig. 8 Menthol synthesis from (±)-citronellal: a) conversion, b) liquid phase mass balance closure, c) total yield, d) yield of menthols. Legend: fresh B – Ru/(H-MCM-41 + Bindzil-50/80), *in situ* synthesis (I, dark blue diamond); reused II B – Ru/(H-MCM-41 + Bindzil-50/80), *in situ* synthesis (II, blue diamond); reused III B – Ru/(H-MCM-41 + Bindzil-50/80), *in situ* synthesis (III, light blue diamond).
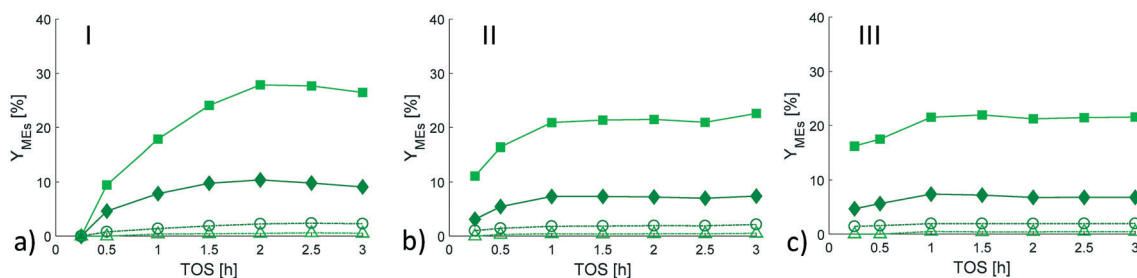
Fig. 9 Menthol isomers as a function of time-on-stream in menthol synthesis from (±)-citronellal over: a) fresh B – Ru/(H-MCM-41 + Bindzil-50/80), *in situ* synthesis; b) reused II B – Ru/(H-MCM-41 + Bindzil-50/80), *in situ* synthesis; c) reused III B – Ru/(H-MCM-41 + Bindzil-50/80), *in situ* synthesis. Legend: menthol (ME, light green, filled square), neomenthol (NME, dark green, filled diamond), isomenthol (IME, light green, empty triangle), neoisomenthol (NIME, dark green, empty circle).

and *p*-menthane were comparable with the yields obtained after the first catalyst reuse (Fig. S9†). The ratios of menthol isomers (Fig. 9 and Table S8†) and isopulegol isomers (Fig. S10 and Table S9†) over reused catalysts (B[II,III]) were comparable with the ratios obtained over the fresh catalyst. No leaching of the fresh or reused catalysts could be detected by ICP-OES analysis.

In the literature,[22] a very similar conversion and the liquid phase mass balance was achieved after the first consecutive use of Ru/H-Beta-300 extrudates without a binder in the citronellal transformations at 35 °C and 10 bar H_2. As in the current case, only washing with a solvent was used for regeneration. Moreover, 3% Ni/Zr-Beta and Zr-Beta & 3% Ni/ MCM-41 catalysts were recycled by calcination at 540 °C for 4 h followed by reduction in H_2.[9] In line with the current work, the results showed that citronellal conversion was unchanged, while the yield of menthols decreased slightly (by

ca. 4%) after three cycles. A decrease in ability of nickel to hydrogenate isopulegols into menthols was explained by sintering of the nickel crystallites because of exposure to high temperatures during calcination and reduction.[9]

4. Conclusions

Four shaped Ru/H-MCM-41-Bindzil catalysts differing in the metal location were prepared by varying the synthesis steps. Menthol synthesis from isopulegol, citronellol and (±)-citronellal (70 °C, 10 bar of H_2) was selected as a model reaction. Different synthesis procedures resulted in the controlled metal deposition in the shaped catalysts in different location and different metal-to-acid site ratio. On the contrary, the concentration of Brønsted and Lewis acid sites and textural properties of the final extrudates were

comparable. The cluster size of Ru particles was in the range from 7 to 13 nm.

In all cases, the transient period indicating a stabilization of the adsorption–desorption equilibrium on the catalyst up to 1.5–2 h of time-on-stream was observed. In (±)-citronellal transformations, it was clearly seen that controlled metal deposition in extrudates has a significant effect on selectivity and activity. While the ratio of the menthol isomers was the same for all catalysts, the ratio of the isopulegol isomers was significantly different and changed with time on stream. Over the catalyst, where Ru was deposited on the catalytic support, (±)-neoisopulegol was unexpectedly obtained as the predominant isomer with 73% stereoselectivity. Formation of individual isopulegols, as well as their total amount, were correlated with the metal-to-acid site ratio and with the yield of menthols. p-Menthane was observed as an intermediate with the maximum up to 1 h of TOS for all type of catalysts.

Compared to other catalysts, a significantly higher amount of acyclic hydrogenated products (citronellol, 3,7-dimethyloctan-1-ol, 2,6-dimethyloctane) was obtained over extrudates of the egg-shell type. This can be attributed to the highest metal-to-acid site ratio and a shorter diffusion distance, as the active metal is concentrated on the outermost layer of the extrudates.

Stereoselectivity to the desired (±)-menthol was 68–70%. The highest amount of the desired menthol (32% yield) was obtained over extrudates where Ru was deposited on the catalytic support, i.e. with the shortest distance between the acid and metal sites, the lowest Brønsted acidity, the lowest Brønsted–Lewis acid sites ratio, the highest specific surface area and the narrowest range of the Ru particle size distribution. Comparison with batch experiments confirmed presence of mass transfer limitations for the extrudates, which, however, did not have an insignificant effect on selectivity except for isopulegol isomers. A consecutive reuse of the extruded catalyst demonstrated catalyst stability, as (±)-citronellal conversion was almost the same, while the yield of isopulegols increased at the expense of menthols. No leaching of the fresh or reused catalysts was observed.

Conflicts of interest

There are no conflicts of interest to declare.

Acknowledgements

References

1 A. Zuliani, C. M. Cova, R. Manno, V. Sebastian, A. A. Romero and R. Luque, Green Chem., 2020, 22, 379–387.

2 J. Plösser, M. Lucas, J. Wärna, T. Salmi, D. Y. Murzin and P. Claus, Org. Process Res. Dev., 2016, 20, 1647–1653.

3 J. Plösser, M. Lucas and P. Claus, J. Catal., 2014, 320, 189–197.

4 The Cool Freshness of Menthol: BASF's Innovative Process for Resource-Efficient Production of the World's Most Popular Flavor, https://www.basf.com/us/en/media/science-around-us/the-cool-freshness-of-menthol.html (accessed June 21, 2020).

5 A. K. Shah, G. Maitlo, A. A. Shah, I. A. Channa, G. A. Kandhro, H. A. Maitlo, U. H. Bhatti, A. Shah, A. Q. Memon, A. S. Jatoi and Y. H. Park, React. Kinet., Mech. Catal., 2019, 128, 1–18.

6 P. Mäki-Arvela, N. Kumar, D. Kubicka, A. Nasir, T. Heikkilä, V. P. Lehto, R. Sjöholm, T. Salmi and D. Y. Murzin, J. Mol. Catal. A: Chem., 2005, 240, 72–81.

7 K. A. da Silva, P. A. Robles-Dutenhefner, E. M. B. Sousa, E. F. Kozhevnikova, I. V. Kozhevnikov and E. V. Gusevskaya, Catal. Commun., 2004, 5, 425–429.

8 P. Mertens, F. Verpoort, A. N. Parvulescu and D. de Vos, J. Catal., 2006, 243, 7–13.

9 Y. T. Nie, W. Niah, S. Jaenicke and G. K. Chuah, J. Catal., 2007, 248, 1–10.

10 P. Mäki-Arvela, N. Kumar, V. Nieminen, R. Sjöholm, T. Salmi and D. Y. Murzin, J. Catal., 2004, 225, 155–169.

11 F. Neatu, S. Coman, V. I. Parvulescu, G. Poncelet, D. de Vos and P. Jacobs, Top. Catal., 2009, 52, 1292–1300.

12 C. B. Cortes, V. T. Galvan, S. S. Pedro and T. V. Garcia, Catal. Today, 2011, 172, 21–26.

13 E. D. Iftitah, M. Muchalal, W. Trisunaryanti and R. Armunanto, Indones. J. Chem., 2010, 10, 201–206.

14 M. Misono and N. Nojiri, Appl. Catal., 1990, 64, 1–30.

15 M. Fuentes, J. Magraner, C. de Las Pozzas and R. Roque-Malherbe, Appl. Catal., 1989, 47, 367–374.

16 A. M. Balu, J. M. Campelo, R. Luque and A. A. Romero, Org. Biomol. Chem., 2010, 8, 2845–2849.

17 E. D. Iftitah, W. T. Muchalal and R. Armunanto, Int. J. Sci. Basic Appl. Res., 2010, 1, 777–781.

18 C. Milone, C. Gangemi, G. Neri, A. Pistone and S. Galvagno, Appl. Catal., A, 2000, 199, 239–244.

19 K. A. D. Rocha, P. A. Robles-Dutenhefner, E. M. B. Sousa, E. F. Kozhevnikova, I. V. Kozhevnikov and E. V. Gusevskaya, Appl. Catal., A, 2007, 317, 171–174.

20 N. Ravasio, N. Poli, R. Psaro, M. Saba and F. Zaccheria, Top. Catal., 2000, 13, 195–199.

21 F. Iosif, S. Coman, V. Parvulescu, P. Grange, S. Delsarte, D. de Vos and P. Jacobs, Chem. Commun., 2004, 1292–1293.

22 M. Azkaar, P. Mäki-Arvela, Z. Vajglová, V. Fedorov, N. Kumar, L. Hupa, J. Hemming, M. Peurla, A. Aho and D. Y. Murzin, React. Chem. Eng., 2019, 4, 2156–2169.

23 C. M. Cova, A. Zuliani, R. Manno, V. Sebastian and R. Luque, Green Chem., 2020, 22, 1414–1423.

24 Z. Vajglová, N. Kumar, M. Peurla, J. Peltonen, I. Heinmaa and D. Y. Murzin, Catal. Sci. Technol., 2018, 8, 6150–6162.

25 Z. Vajglová, N. Kumar, P. Mäki-Arvela, K. Eränen, M. Peurla, L. Hupa and D. Y. Murzin, Org. Process Res. Dev., 2019, 23, 2456–2463.

26 Z. Vajglová, N. Kumar, M. Peurla, L. Hupa, K. Semikin, D. A. Sladkovskiy and D. Y. Murzin, *Ind. Eng. Chem. Res.*, 2019, **58**, 10875–10885.

27 Z. Vajglová, N. Kumar, P. Mäki-Arvela, K. Eränen, M. Peurla, L. Hupa, M. Nurmi, M. Toivakka and D. Y. Murzin, *Ind. Eng. Chem. Res.*, 2019, **58**, 18084–18096.

28 P. S. F. Mendes, J. M. Silva, M. F. Ribeiro, A. Daudin and C. Bouchy, *J. Ind. Eng. Chem.*, 2018, **62**, 72–83.

29 G. T. Whiting, F. Meirer, M. M. Mertens, A. J. Bons, B. M. Weiss, P. A. Stevens, E. de Smit and B. M. Weckhuysen, *ChemCatChem*, 2015, **7**, 1312–1321.

30 R. V. Jasra, B. Tyagi, Y. M. Badheka, V. N. Choudary and T. S. G. Bhat, *Ind. Eng. Chem. Res.*, 2003, **42**, 3263–3272.

31 F. Dorado, R. Romero and P. Canizares, *Ind. Eng. Chem. Res.*, 2001, **40**, 3428–3434.

32 H. Liu, Y. M. Zhou, Y. W. Zhang, L. Y. Bai and M. H. Tang, *Ind. Eng. Chem. Res.*, 2008, **47**, 8142–8147.

33 M. B. Yue, N. Yang and Y. M. Wang, *Wuli Huaxue Xuebao*, 2012, **28**, 2115–2121.

34 Y. Song, L. L. Zhang, G. D. Li, Y. S. Shang, X. M. Zhao, T. Ma, L. M. Zhang, Y. L. Zhai, Y. J. Gong, J. Xu and F. Deng, *Fuel Process. Technol.*, 2017, **168**, 105–115.

35 X. Wu, A. Alkhawaldeh and R. G. Anthony, Investigation on Acidity of Zeolites Bound with Silica and Alumina, in *Studies in Surface Science and Catalysis*, Elsevier Science, 2002, pp. 217–225.

36 G. D. Yadav and J. J. Nair, *Langmuir*, 2000, **16**, 4072–4079.

37 A. F. Trasarti, A. J. Marchi and C. R. Apesteguia, *J. Catal.*, 2004, **224**, 484–488.

38 A. F. Trasarti, A. J. Marchi and C. R. Apesteguia, *J. Catal.*, 2007, **247**, 155–165.

39 I. L. Simakova, Y. S. Demidova, M. N. Simonov, P. S. Niphadkar, V. V. Bokade, N. Devi, P. L. Dhepe and D. Y. Murzin, *Catal. Sustainable Energy*, 2019, **6**, 38–49.

40 C. A. Emeis, *J. Catal.*, 1993, **141**, 347–354.

41 G. Mary, A. Esmaeili and J. Chaouki, *Int. J. Chem. React. Eng.*, 2016, **14**, 859–874.

42 M. I. Urseanu, J. G. Boelhouwer, H. J. M. Bosman, J. C. Schroijen and G. Kwant, *Chem. Eng. J.*, 2005, **111**, 5–11.

43 J. T. Dam, A. Ramanathan, K. Djanashvili, F. Kapteijn and U. Hanefeld, *RSC Adv.*, 2017, **7**, 12041–12053.

44 Y. Z. Zhu, Y. T. Nie, S. Jaenicke and G. K. Chuah, *J. Catal.*, 2005, **229**, 404–413.

This journal is © The Royal Society of Chemistry 2020

Catal. Sci. Technol., 2020, **10**, 8108–8119 | **8119**